A Hybrid Nonlinear Active Noise Control Method Using Chebyshev Nonlinear Filter

Bin Chen[1, *], Shuyue Yu[1], Yan Gao[2]

[1] School of Automation, Beijing University of Posts and Telecommunications, Beijing, 100876, China

[2] Key Laboratory of Noise and Vibration Research, Institute of Acoustics, Chinese Academy of Sciences, Beijing, 100190, China

Investigations into active noise control (ANC) technique have been conducted with the aim of effective control of the low-frequency noise. In practice, however, the performance of currently available ANC systems degrades due to the effects of nonlinearity in the primary and secondary paths, primary noise and louder speaker. This paper proposes a hybrid control structure of nonlinear ANC system to control the non-stationary noise produced by the rotating machinery on the nonlinear primary path. A fast version of ensemble empirical mode decomposition is used to decompose the non-stationary primary noise into intrinsic mode functions, which are expanded using the second-order Chebyshev nonlinear filter and then individually controlled. The convergence of the nonlinear ANC system is also discussed. Simulation results demonstrate that proposed method outperforms the FSLMS and VFXLMS algorithms with respect to noise reduction and convergence rate.

1 Introduction

Active noise control (ANC) is based on the principle of destructive interference by generating an anti-noise with the same amplitude but inverse phase of the noise. The linear finite impulse response (FIR) filter with the filtered-x least mean square (FxLMS) algorithm is widely used for conventional ANC systems[1]. However, difficulties of the nonlinearities are often encountered in the primary and secondary paths, primary noise or the louder speaker system[2]. As a result, the performance of the ANC system degrades with respect to convergence rate and noise reduction. The adaptive filters, such as Volterra filter[2-6], functional link artificial neural network (FLANN)[7-12], and even mirror Fourier nonlinear (EMFN) filter[13-14], have been designed and implemented in the ANC systems.

Tan and Jiang[2] designed a Volterra filtered-x LMS (VFXLMS) algorithm for the non-minimum phase of the secondary path, which achieved better performance compared to the standard FxLMS. Since this first study, many computationally efficient Volterra filters have been presented for nonlinear ANC systems[3-5]. To overcome the impulse noise in the nonlinear ANC system, Lu and Zhao[6] developed a Volterra expansion model by minimizing the lp-norm of the logarithmic cost. The Volterra filter requires a large number of multi-dimensional coefficients for accurately modeling nonlinear systems, which has a large computational complexity. Only the second-order Volterra and third-order Volterra filters have been successfully applied in practical applications.

To reduce the computational cost, Das and Panda[7] proposed a novel filtered-s least mean square (FSLMS) algorithm using the FLANN structure. Some modified FLANN filters were then developed to improve the learning process, such as reduced feedback FLANN[8], nonlinear neuro-controller based FLANN[9], recursive FLANN[10] and convex combination of two FLANN filters[11]. Nevertheless, the cross-terms, i.e. products of samples with different time delays were not

taken into account in their work[7-11]. Sicuranza and Carini[12] proposed a generalized FLANN (GFLANN) by adding appropriate cross-terms to the FLANN filter. It is noted that the basis functions of FLANN and GFLANN filters do not satisfy the condition of the well-known Stone-Weierstrass approximation theorem[15]. Recently, the EMFN filter has been proposed and applied to the nonlinear ANC system, which can achieve better convergence rate and lower approximation error in presence of the strong nonlinearities[13-14]. The Chebyshev nonlinear (CN) filter, deduced by Alberto and Giovanni[16], is a product of the first kind Chebyshev polynomial expansions of the input samples. It satisfies the requirement of the Stone-Weierstrass approximation theorem, which is suitable for any causal, time-invariant, finite-memory, continuous and nonlinear systems.

This paper describes a hybrid control structure of nonlinear ANC system. It introduces the CN filter to control the non-stationary noise produced by rotating machinery on the nonlinear primary path. First of all, a fast version of ensemble empirical mode decomposition (EEMD)[17] is used to decompose the non-stationary primary noise into intrinsic mode functions (IMFs). The IMFs are individually expanded using the second-order CN filter, the weights of which are updated by the LMS algorithm. It is demonstrated that the proposed algorithm is robust for the non-stationary noise and nonlinear primary path.

The remaining part of the paper is organized as follows. Section 2 presents the principle of proposed algorithm based on the real-time EEMD and adaptive CN filter. A set of simulations have been carried out in Section 3 to evaluate the performance of the proposed nonlinear ANC system. Finally, conclusions are drawn in Section 4.

2 The Proposed Algorithm

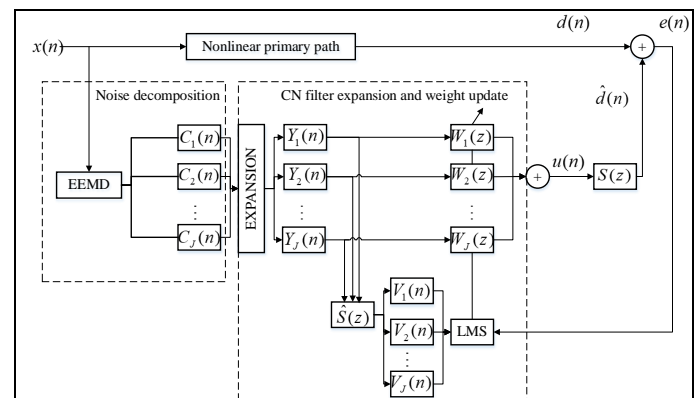### 2.1 Hybrid Control Structure of Nonlinear ANC System

Figure 1. Schematic block diagram of the proposed algorithm.

The basic block diagram of the nonlinear ANC system is shown in Figure 1. It comprises two processes, including noise decomposition using the real-time EEMD, and the CN filter expansion and weight update. In the figure, $x(n)$ denotes the primary noise; $u(n)$ denotes the output of the adaptive CN filters; $e(n)$ denotes the error signal;

$S(z)$ represents the transfer function of the secondary path; $\hat{S}(z)$ represents the estimate of the secondary path; $C_j(n)$ are the decomposed IMFs; $V_j(n)$ are the filtered vectors of $Y_j(n)$ through secondary path estimate $\hat{S}(z)$. The primary noise after passing through the nonlinear primary path is denoted as reference noise $d(n)$, and the output $u(n)$ after passing through the secondary path is referred to as secondary noise $\hat{d}(n)$.

2.2 Nonlinear Primary Path Model

Block-oriented model, consisting of a linear time-invariant (LTI) block and a static nonlinear block, is the most popular representation of nonlinear systems. This method reduces the number of coefficients and the size of the required memory. Figure 2 shows three types of Wiener, Hammerstein and LNL models[3]. In the ANC system, the LTI block is expressed by finite-impulse-response (FIR) filter, while the nonlinearity can be represented by a polynomial with fixed memoryless nonlinear function.
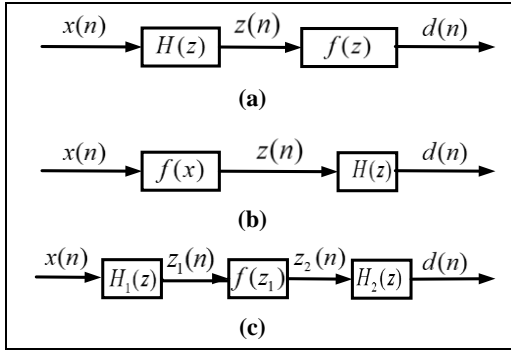

Figure 2. Nonlinear primary path models: (a) Wiener (b) Hammerstein (c) LNL.

As shown in Figure 2(a), the Wiener system consists of a LTI block followed by a static nonlinear block, expressed by

$$z(n) = \sum_{i=1}^{H} h_i(n)x(n-i+1) \tag{1}$$

$$d(n) = f(z(n)) \tag{2}$$

where $x(n)$ is the primary noise; $z(n)$ is the output of FIR filter; $d(n)$ is the reference noise; H denotes order of the FIR filter; $h_i(n)$ denotes FIR filter coefficients; $f(\cdot)$ denotes a nonlinear function.

The Hammerstein system, shown in Figure 2(b), reverses the order of LTI and static nonlinear blocks in Wiener-based model, denoted by

$$z(n) = f(x(n)) \tag{3}$$

$$d(n) = \sum_{i=1}^{H} h_i(n)z(n-i+1) \tag{4}$$

The LNL system is a series connection of the Wiener and Hammerstein, with a static nonlinearity sandwiched between two LTI blocks, shown in Figure 2(c), given by

$$z_1(n) = \sum_{i=1}^{H_1} h_{1,i}(n)x(n-i+1) \tag{5}$$

$$z_2(n) = f(z_1(n)) \tag{6}$$

$$d(n) = \sum_{i=1}^{H_2} h_{2,i}(n)z_2(n-i+1) \tag{7}$$

The nonlinear block is a continuous function expressed by Taylor expansion[18], and the output of which is given by

$$z(n) = \sum_{t=1}^{T} \left[a_{t,0}x(n) + a_{t,1}x(n-1) + \cdots + a_{t,m}x(n-m) \right]^t$$
$$= \sum_{t=1}^{T} \left[\sum_{t_1=0}^{t} \sum_{t_2=0}^{t_1} \cdots \sum_{t_m=0}^{t_{m-1}} \left(\frac{t!}{t_m!(t-t_1)! \cdots (t_{m-1}-t_m)!} \right) \left(a_{t,0}x(n) \right)^{t-t_1} \left(a_{t,1}x(n-1) \right)^{t_1-t_2} \cdots \left(a_{t,m}x(n-m) \right)^{t_m} \right] \tag{8}$$

where $T \in N^*$ is an order. If $T > 1$, the primary path is nonlinear; otherwise, it is linear.

The roller bearing is one of the key elements in rotating machinery. The generated noise becomes much more non-stationary under variable speed, especially for startup and shutdown, which can be expressed as

$$x_s(n) = \sum_q B_q \cos(2\pi q f_s n + \beta_q) \tag{9}$$

where f_s is a rotational frequency of the shaft; B_q and β_q are amplitude and initial phase of the q-th harmonic.

Substituting Equation (9) into the power function $(\cdot)^k$ leads to when $q=1, k=2$

$$x_s^2(n) = \frac{B_1^2}{2} \cos(2\pi \cdot 2 f_s \cdot n + 2\beta_1) + \frac{B_1^2}{2} \tag{10}$$

when $q=1, k=3$

$$x_s^3(n) = \frac{B_1^3}{4} \cos(2\pi \cdot 3 f_s \cdot n + 3\beta_1) + \frac{3B_1^3}{4} \cos(2\pi \cdot f_s \cdot n + \beta_1) \tag{11}$$

when $q=1, k=4$

$$x_s^4(n) = \frac{B_1^4}{8} \cos(2\pi \cdot 4 f_s \cdot n + 4\beta_1) + \frac{B_1^4}{2} \cos(2\pi \cdot 2 f_s \cdot n + 2\beta_1) + \frac{3B_1^4}{8} \tag{12}$$

The analytical expressions are obtained by

$$x_s^k(n) = \begin{cases} \sum_{i=1}^{I} d_{k,i} \cos\left(2\pi \cdot (k-2i+2)f_s \cdot n + (k-2i+2)\beta_1\right) & \text{if } k = 2I - 1 \\ \sum_{i=1}^{I} d_{k,i} \cos\left(2\pi \cdot (k-2i+2)f_s \cdot n + (k-2i+2)\beta_1\right) + d_{k,0} & \text{if } k = 2I \end{cases} \tag{13}$$

where $i = 1, 2, \cdots, I$, $k \in N^*$; $d_{k,i}$ are amplitudes of the harmonics; $d_{k,0}$ are constant terms.

Similarly, when $q > 1$, analytical expressions are given by

$$x_s^k(n) = \sum_{i=1}^{I'} d'_{k,i} \cos(2\pi \cdot i f_s \cdot n + \beta_{k,i}) + d'_{k,0} \tag{14}$$

where $i = 1, 2, \cdots, I'$, $I' = q \cdot k$, $k \in N^*$; $d'_{k,i}$ are the amplitudes of the harmonics; $d'_{k,0}$ are constant terms. Substituting Equation (14) into Equation (8) leads to the output signal given by

$$z(n) = \sum_{i=1}^{I'} g_{k,i} \cos(2\pi \cdot i f_s \cdot n + \beta_{k,i}) + \gamma(n) \tag{15}$$

where $\gamma(n)$ is a constant term. Compared to the primary noise, $x_s(n)$, it is found that the frequency components of the output signal passed through the nonlinear primary path contain some higher order harmonics.

2.3 Noise Decomposition

The EEMD is a popular method in the analysis of the non-stationary primary noise. Partition the data series of primary noise into windows, each sub-series thus would be processed by EEMD, sequentially, from left to right. The choice of the window length needs to satisfy the following two conditions: (a) Sufficiently long to result in reasonably stationary IMFs; (b) Short enough to ensure a shorter delay and fast response to the primary noise. Appropriate length can be adjusted in the experiments. The procedures are as follows:

(1) Initialize the number of trials K, the amplitude of the added white noise, and set the trial number $i = 1$. The generated white noise series

$n_i(n)$ is added to the primary noise to obtain the i-th trial by

$$x_i(n) = x(n) + n_i(n) \tag{16}$$

(2) Decompose the noise-added signal into IMFs with the EMD as

$$x_i(n) = \sum_{j=1}^{J} \upsilon_{i,j}(n) + r_{i,J}(n) \tag{17}$$

where $i = 1, 2, ..., K$, $j = 1, 2, ..., J$; $\upsilon_{i,j}$ denotes the j-th IMF of the i-th trial; $r_{i,J}(n)$ is a residue of the signal; J denotes the total number of the decomposed IMFs by

$$J = fix(\log_2(N_W)) \tag{18}$$

where $fix(\cdot)$ is an integral function; N_W denotes a length of the window.

(3) Repeat the EMD decomposition K times with random white noise to lead to an ensemble of IMFs. Finally, the j-th IMF is calculated by

$$IMF_j = \frac{1}{K} \sum_{i=1}^{K} \upsilon_{i,j} \tag{19}$$

2.4 Weight Update

To overcome the nonlinearity existing in the primary path, the IMFs are expanded using the CN filter based on the Chebyshev polynomial, which is a family of orthogonal polynomials generated by the following recursive relation

$$T_{n+1}(x) = 2 \cdot x \cdot T_n(x) + T_{n-1}(x) \tag{20}$$

where $T_n(x)$ is the Chebyshev polynomial of order n. For example, $T_0(x) = 1$, $T_1(x) = x$, $T_2(x) = 2x^2 - 1$, $T_3(x) = 4x^3 - 3x$, $T_4(x) = 8x^4 - 8x^2 + 1$ and $T_5(x) = 16x^5 - 20x^3 + 5x$.

For the j-th IMF $C_j(n) = [c_j(n), c_j(n-1), ..., c_j(n-N+1)]^T$, the expanded signal with a second-order CN filter is given by

$$
\begin{aligned}
Y_j(n) &= \left[y_{j,0}(n), y_{j,1}(n), y_{j,2}(n), \ldots y_{j,Q-1}(n) \right]^T \\
&= \{ T_0[c_j(n)], T_0[c_j(n-1)], \cdots, T_0[c_j(n-N+1)], \\
&\quad T_1[c_j(n)], T_1[c_j(n-1)], \cdots, T_1[c_j(n-N+1)], \\
&\quad T_2[c_j(n)], T_2[c_j(n-1)], \cdots, T_2[c_j(n-N+1)], \\
&\quad T_1[c_j(n)]T_1[c_j(n-1)], ..., T_1[c_j(n-N+2)]T_1[c_j(n-N+1)], \\
&\quad T_1[c_j(n)]T_1[c_j(n-2)], \cdots, T_1[c_j(n-N+3)]T_1[c_j(n-N+1)], \\
&\quad \ldots \ldots \\
&\quad T_1[c_j(n)]T_1[c_j(n-N+1)] \}^T
\end{aligned}
\tag{21}
$$

where Q is the length of expanded signal.

The output of j-th IMF controller is a convolution of the expanded signal and impulse response. The sum of all controllers is taken as an input of the louder speaker, given by

$$u(n) = \sum_{j=1}^{J} W_j^T(n) Y_j(n) \tag{22}$$

where the weight vector $W_j(n) = \left[w_{j,0}(n), w_{j,1}(n), ..., w_{j,Q-1}(n) \right]^T$.

The error signal measured at the error microphone is a summation of reference noise and secondary noise by

$$e(n) = d(n) + \hat{d}(n) \tag{23}$$

with the secondary noise given by

$$
\begin{aligned}
\hat{d}(n) &= s(n) * u(n) = \sum_{l=0}^{L-1} s_l(n) u(n-l) \\
&= \sum_{l=0}^{L-1} s_l(n) \sum_{j=1}^{J} \sum_{i=0}^{Q-1} w_{j,i}(n-l) y_j(n-i-l) \\
&= \sum_{j=1}^{J} \sum_{i=0}^{Q-1} w_{j,i}(n) \sum_{l=0}^{L-1} s_l(n-i) y_j(n-i-l)
\end{aligned}
\tag{24}
$$

where $s(n)$ is an impulse response of the transfer function of the secondary path $S(z)$

$$S(z) = s_0 + s_1 z^{-1} + s_2 z^{-2} + s_3 z^{-3} + \cdots s_{L-1} z^{-L+1} \tag{25}$$

where z^{-1} denotes a unit delay; L is an order of secondary path.

Assumed the estimated secondary path $\hat{S}(z)$ is the same as secondary path $S(z)$, the error signal is simplified as

$$e(n) = d(n) + \sum_{j=1}^{J} \sum_{i=0}^{Q-1} w_{j,i}(n) v_j(n-i) = d(n) + \sum_{j=1}^{J} W_j^T(n) V_j(n) \tag{26}$$

where $v_j(n) = \sum_{l=0}^{L-1} s_l y_j(n-l)$ and $V_j(n) = \left[v_j(n), v_j(n-1), ..., v_j(n-Q+1) \right]^T$.

The cost function is defined by the mean square error (MSE) of error signal by

$$J(n) = E\left[e^2(n) \right] \tag{27}$$

where $E[\bullet]$ is an expectation operator. The gradient of cost function is obtained by

$$\nabla_j(n) = \frac{\partial J(n)}{\partial W_j} \cong \frac{\partial e^2(n)}{\partial W_j} = 2e(n) \frac{\partial e(n)}{\partial W_j} = 2e(n) V_j(n) \tag{28}$$

Hence, the weight vector is updated using the steepest descent method by

$$W_j(n+1) = W_j(n) - \frac{\mu}{2} \nabla_j(n) = W_j(n) - \mu e(n) V_j(n) \tag{29}$$

where μ is a step-size.

2.5 Convergence Analysis

Substituting Equation (26) into Equation (29), the expectation of the weight vector $W_j(n+1)$ is given by

$$W_j(n+1) = W_j(n) - \mu E\left[d(n) V_j(n) \right] - \mu E\left[\sum_{i=1}^{J} V_j(n) V_i^T(n) \right] W_i(n) \tag{30}$$

According to basic principle of the EEMD, the IMFs are orthogonal. Thus Equation (30) can be simplified as

$$W_j(n+1) = (I - \mu R_j) W_j(n) - \mu P_j \tag{31}$$

where $R_j = E\left[V_j(n) V_j^T(n) \right]$ and $P_j = E\left[d(n) V_j(n) \right]$.

When the ANC system achieves the steady state, $W_j(n+1) \approx W_j(n)$. The optimal weight vector becomes

$$W_j^* = \lim_{n \to \infty} W_j(n) = -R_j^{-1} P_j \tag{32}$$

Subtracting W_j^* from Equation (31), the error of the weight vector is given by

$$\delta_j(n+1) = \left[I - \mu R_j \right] \delta_j(n) = A_j^{-1} \left[I - \mu \Lambda_j \right] A_j \delta_j(n) = A_j^{-1} \left[I - \mu \Lambda_j \right]^{n+1} A_j \delta_j(0) \tag{33}$$

where $\delta_j(n) = W_j(n) - W_j^*$; $R_j = A_j^{-1} \Lambda_j A_j$; $\Lambda_j = diag\left[\lambda_{j,1}, \lambda_{j,2}, \cdots, \lambda_{j,Q} \right]$ is a diagonal matrix composed of the eigenvalues of R_j.

The convergence condition of Equation (33) is $\left| 1 - \mu \lambda_{j\max} \right| < 1$. Thus, the step-size satisfying the convergence and stability of the proposed algorithm is given by

$$0 < \mu < \frac{1}{\lambda_{\max}} \tag{34}$$

where $\lambda_{\max}$ is the maximum eigenvalue.

3 Simulations and Discussions

In this section, some simulations are conducted to demonstrate the effectiveness of the proposed nonlinear ANC structure, in comparison with the VFXLMS algorithm[2] and FSLMS algorithm[7]. The sampling frequency is 3 kHz. The memory sizes of the FLANN, Volterra and

CN filters are chosen as $N = 10$. In the EEMD algorithm, $N_W = 300$, $K = 50$, and the amplitude of the added white noise is set as 0.2 times the standard deviation of primary signal.

The reference noise at the cancellation point is generated based on the following second-order polynomial model given by

$$d(n) = z(n-2) + 0.8z(n-2)z(n-2) + 0.75z(n)z(n-3) \qquad (35)$$

$$H(z) = z^{-5} - 0.3z^{-6} + 0.2z^{-7} \qquad (36)$$

The secondary path transfer function is given by

$$S(z) = z^{-2} + 1.5z^{-3} - z^{-4} \qquad (37)$$

3.1 Case 1

The non-stationary primary noise is generated by using Equation (9). It consists of three shaft harmonics, with amplitudes and phases being of $B_1 = 1.0$, $B_2 = 1.5$, $B_3 = 1.2$, $\beta_1 = \pi/6$, $\beta_2 = -\pi/3$, $\beta_3 = \pi/2$.

The roller bearing experiences a run-up and run-down process with the speed curve given by $f_s = [800 + 200\sin(2\pi \cdot 0.2 \cdot t)]/60$. Random noise is added with a signal-to-noise ratio of 3.7 dB, and the length of primary noise is 10 s. Figure 3 plots the mixed signal with the shaft harmonics and random noise, the STFT spectrogram of which is shown in Figure 4, with the ordinate being 0-100 Hz for better display. Clearly, three distinct harmonics exist in the time-frequency representation, varying with time in terms of the approximate sine.
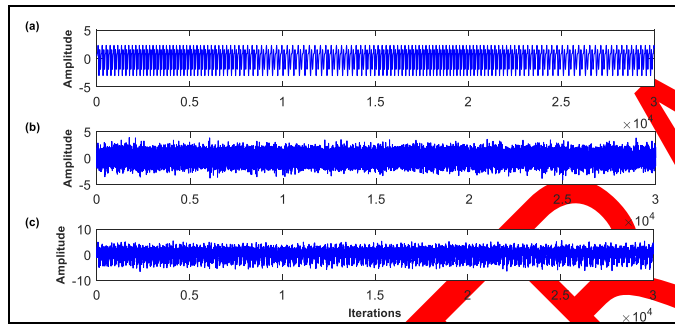

Figure 3. The simulated signal: (a) the shaft harmonics; (b) the random noise; (c) the mixed signal.
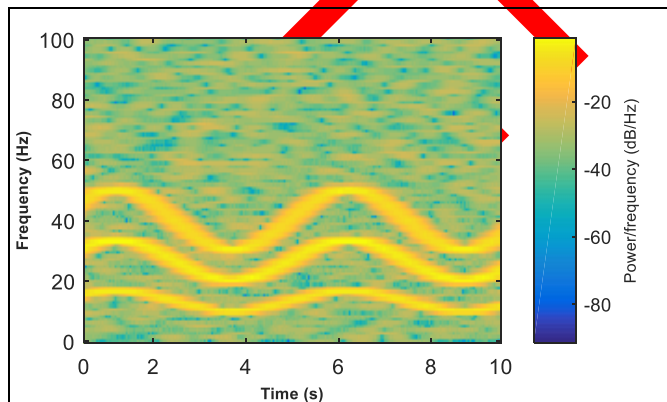

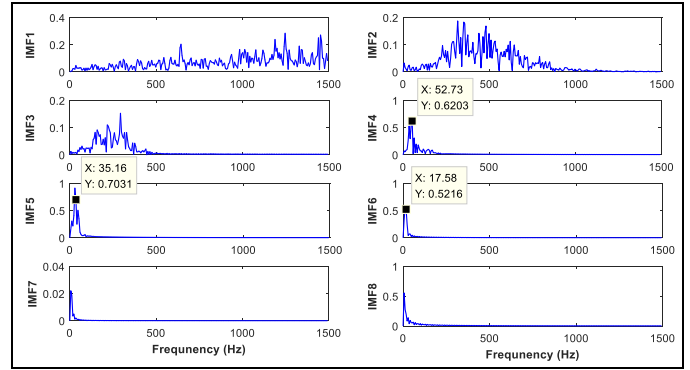*Figure 4. The STFT spectrogram of the mixed signal.*

Figure 5. Spectra of the decomposed IMFs.

Figure 5 shows the spectra of the decomposed IMFs for a computation window of the primary noise from 2701-3000 iterations. Since the EEMD has a property of binary filtering, the frequency band of the IMF is narrowed down with increasing the decomposition level. The third harmonic, second harmonic and fundamental harmonic components are separated from the mixed signal, approximately locating at the IMF4, IMF5 and IMF6 with peak values of 52.73 Hz, 35.16 Hz and 17.58 Hz respectively. In the decomposition process, the IMF becomes more simple and stationary.

Figure 6 shows the error signal and PSD by using the FSLMS, VFXLMS and proposed algorithm with a step-size of 4×10^{-6}. To better discern the curves behavior, the power spectral density (PSD) is obtained by averaging over 20 independent runs and smoothed with a window of length equal to 10 samples. As shown in Figure 6(a), compared to the FSLMS and VFXLMS algorithms, the proposed method exhibits the least residual error in steady-state, and provides a faster convergence rate since the CN filter has orthogonal basis functions for input signal. It can be seen from Figure 6(b), the FSLMS achieves a large reduction of 12.8 dB at 10 Hz near the fundamental harmonic, but ineffective for other frequencies of the primary noise. In comparison, both the VFXLMS and proposed algorithm have a large reduction below 150 Hz in the variation of the shaft harmonics, with the latter having the largest reduction from 25-80 Hz.

Figure 7(a) plots the STFT spectrogram of the primary noise passing through the nonlinear primary path. Clearly, three higher order harmonics appear in comparison of the primary noise. Figures 7(b)-7(d) plot the STFT spectrograms of the error signal canceled by the FSLMS, VFXLMS and proposed algorithm respectively. The FSLMS effectively reduces the primary noise at the fundamental harmonic but inefficient for higher order harmonics. Compared to the FSLMS, the VFXLMS performs better since it exploits cross-terms in the nonlinear expansion with the second-order Volterra filter. It is obvious that the proposed method is effective at all the shaft harmonics and has the most reduction compared to the other algorithms for controlling the non-stationary noise. This suggests that the proposed algorithm is capable of compensating for nonlinear distortions such as the harmonics introduced by the nonlinear primary path.
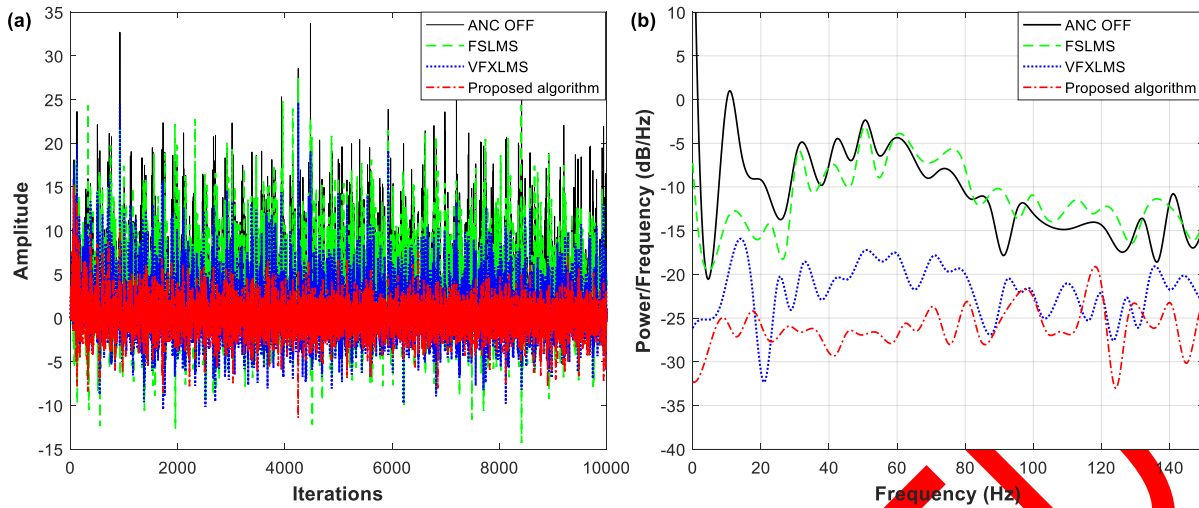
Figure 6. Simulation results for Case 1: (a) error signal; (b) PSD.
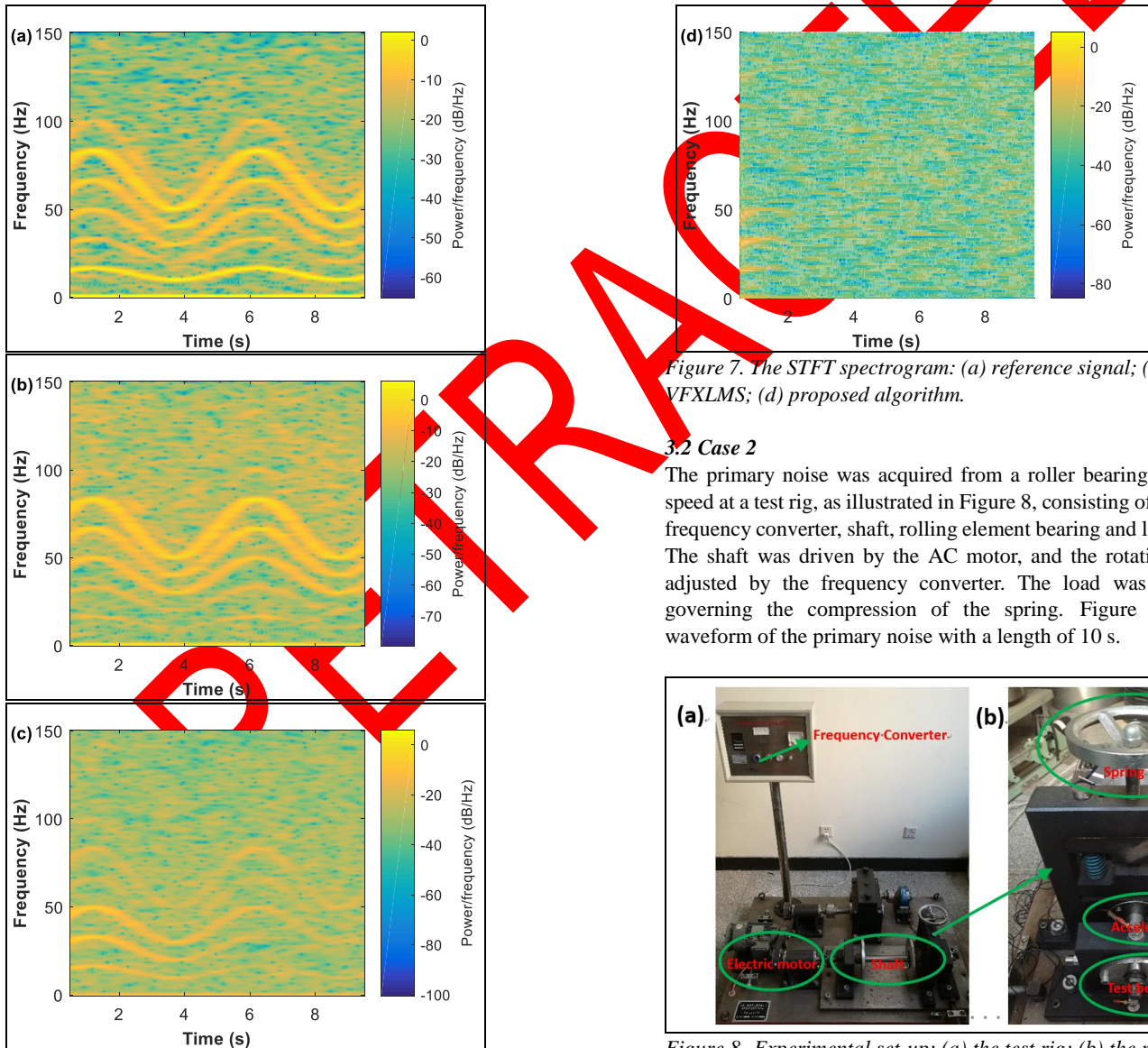

Figure 7. The STFT spectrogram: (a) reference signal; (b) FSLMS; (c) VFXLMS; (d) proposed algorithm.

3.2 Case 2

The primary noise was acquired from a roller bearing under run-up speed at a test rig, as illustrated in Figure 8, consisting of an AC motor, frequency converter, shaft, rolling element bearing and load controller. The shaft was driven by the AC motor, and the rotating speed was adjusted by the frequency converter. The load was regulated by governing the compression of the spring. Figure 9 shows the waveform of the primary noise with a length of 10 s.
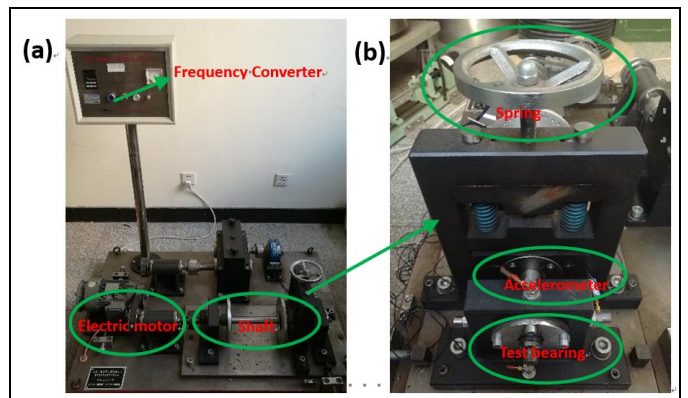

Figure 8. Experimental set-up: (a) the test rig; (b) the rolling element bearing.
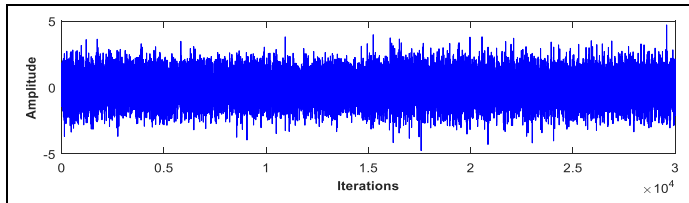
Figure 9. The waveform of the non-stationary noise.

The waveform and STFT spectrogram of the primary noise is shown in Figure 10. Obviously, the signal varies with time and has a characteristic of non-stationarity, containing some distinct shaft harmonics. Moreover, these harmonics approximately increase in a constant acceleration with time.
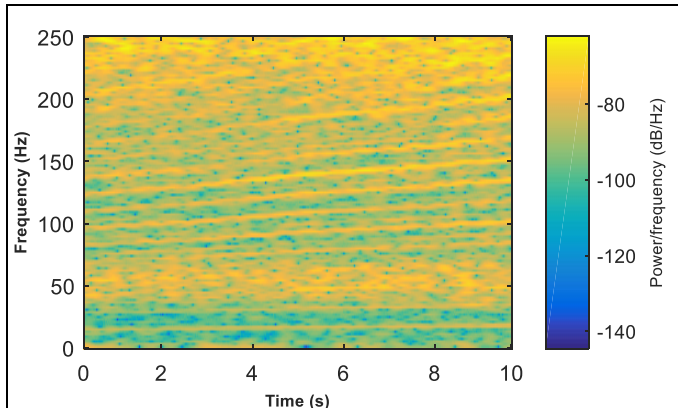

Figure 10. The STFT spectrogram of the non-stationary noise.

Figure 11 shows the results of error signal and PSD by using the FSLMS, VFXLMS and proposed algorithm with a step-size of 1×10^{-5}. The noise reduction of three methods in the entire frequency band is shown in Table 1. The VFXLMS has a reduction of 0.032 dB for the non-stationary primary noise, while the FSLMS exhibits a slightly better performance at some frequencies with a reduction of 0.788 dB. The proposed algorithm can cancel the non-stationary noise to a greater extent on the nonlinear primary path, with more reductions of 3.107 dB and 3.863 dB compared to the FSLMS and VFXLMS. Besides, it provides the fastest convergence rate through about 4000 iterations to reach the steady-state.
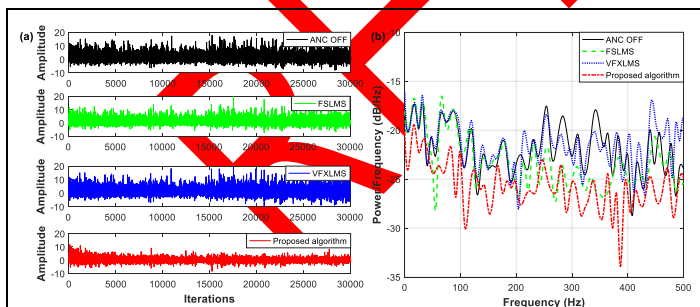

Figure 11. Simulation results for Case 2: (a) error signal; (b) PSD.

Table 1. Noise reduction of different methods (dB).

Algorithm	FSLMS	VFXLMS	Proposed method
Overall frequency band	0.788	0.032	3.895

4 Conclusion

This paper proposes a new algorithm based on the adaptive CN filter and EEMD for active control of the non-stationary primary noise on the nonlinear primary path. It has been shown that the noise becomes more stable and easily controlled by using the real-time EEMD decomposition. The adaptive CN filter has been demonstrated to accurately model the nonlinear primary path than the FLANN and Volterra filters. Simulations have been carried out to show that the proposed algorithm outperforms the FSLMS and VFXLMS in noise reduction and convergence rate.

References

1. Schirmacher, R., "Current status and future developments of ANC systems," Sound and Vibration, Vol. 50, No. 9, pp. 16-19, 2016.
2. Tan L., Jiang J., "Adaptive Volterra filters for active control of nonlinear noise processes," IEEE Transactions on Signal Processing, Vol. 49, No. 8, pp. 1667-1676, 2001.
3. Zhou, D. Y., Brunner, V. D., "Efficient adaptive nonlinear filters for nonlinear active noise control," IEEE Transactions on Circuits and Systems, Vol. 54, No. 3, pp. 669-681, 2007.
4. Zhao, H., Zeng, X., Zhang, X., He, Z., Li, T. et al., "Adaptive extended pipelined second-order Volterra filter for nonlinear active noise controller," IEEE Transactions on Audio, Speech, and Language Processing, Vol. 20, No. 4, pp. 1394-1399, 2012.
5. Zhao, H. Q., Zeng, X. P., He, Z. Y., Li, T. R., "Adaptive RSOV filter using the FELMS algorithm for nonlinear active noise control systems," Mechanical Systems and Signal Processing, Vol. 34, pp. 378-392, 2013.
6. Lu, L., Zhao, H. Q., "Adaptive Volterra filter with continuous *lp*-norm using a logarithmic cost for nonlinear active noise control," Journal of Sound and Vibration, Vol. 364, pp. 14-29, 2016.
7. Das, D. P., Panda, G., "Active mitigation of nonlinear noise processes using a novel filtered-s LMS algorithm," IEEE Transactions Speech and Audio Processing, Vol. 12, No. 3, pp. 313-322, 2004.
8. Zhao, H. Q., Zeng, X. P., Zhang, J. S., "Adaptive reduced feedback FLNN filter for active noise control of nonlinear noise processes," Signal Processing, Vol. 90, pp. 834-847, 2010.
9. Zhang, X., Ren, X., Na, J., Zhang, B., Huang, H., "Adaptive nonlinear neuro-controller with an integrated evaluation algorithm for nonlinear active noise systems," Journal of Sound and Vibration, Vol. 329, pp. 500-5016, 2010.
10. Sicuranza, G. L., Carini, A., "On the BIBO stability condition of adaptive recursive FLANN filters with application to nonlinear active noise control," IEEE Transactions on Audio, Speech, and Language Processing, Vol. 20, No. 1, pp. 234-245, 2012.
11. Zhao, H. Q., Zeng, X. P., He, Z. Y., Yu, S. J., Chen, B. D., "Improved functional link artificial neural network via convex combination for nonlinear active noise control," Applied Soft Computing, Vol. 42, pp. 351-359, 2016.
12. Sicuranza, G. L., Carini, A., "A generalized FLANN filter for nonlinear active noise control," IEEE Transactions on Audio, Speech, and Language Processing, Vol. 19, No. 8, pp. 2412-2417, 2011.
13. Carini, A., Sicuranza, G. L., "Even mirror Fourier nonlinear filters," Proceedings of ICASSP 2013, International Conference

on Acoustic, Speech, Signal Processing, Vancouver, Canada, May 2013.

14. Patel, V., George, N. V., "Partial update even mirror Fourier non-linear filters for active noise control," Proceedings of the 23rd European signal processing conference (EUSIPCO), Nice, France, August 2015.

15. Rudin, W., "Principles of Mathematical Analysis," New York: McGraw-Hill, 1976.

16. Carini, A., Sicuranza, G. L., "A study about Chebyshev nonlinear filters," Signal Processing, Vol. 122, pp. 24-32, 2016.

17. Wu, Z. H., Huang, N. E., "Ensemble empirical mode decomposition: a noise-assisted data analysis method," Advances in adaptive data analysis, Vol. 1, pp. 1-41, 2009.

18. Luo, L., Sun, J. W., Huang, B. Y., "Efficient combination of feedforward and feedback structures for nonlinear narrowband active noise control," Signal Processing, Vol. 128, pp. 494-503, 2016.

The author can be reached at: binchen@bupt.edu.cn.